Journal of Materials Chemistry A

PAPER

View Article Online
View Journal | View Issue

Check for updates

Cite this: J. Mater. Chem. A, 2019, 7, 7082

High-performance carbon molecular sieve membranes for hydrogen purification and pervaporation dehydration of organic solvents†

P. H. Tchoua Ngamou, *[ab] M. E. Ivanova, [ab] O. Guillon [ab] and W. A. Meulenberg [abc]

Received 1st October 2018
Accepted 28th February 2019

DOI: 10.1039/c8ta09504c

rsc.li/materials-a

Ultrathin (~200 nm) and defect-free carbon molecular sieve (CMS) membranes were successfully fabricated on the inner surface of hierarchically structured porous supports (γ-Al_2O_3 layer coated α-Al_2O_3 tubes) *via* pyrolysis of a polyimide precursor at 700 °C. The chemical structure of the carbonized samples was examined in detail by means of Raman spectroscopy and X-ray photoelectron spectroscopy. From these studies, it was found that the carbonized samples consist of graphitic carbon layers containing sp^3-type defects. The synthesized CMS membranes showed an unprecedentedly high H_2 permeance of up to 1.1×10^{-6} mol m^{-2} s^{-1} Pa^{-1} and ideal separation factors of 24, 130 and 228 for H_2/CO_2, H_2/N_2 and H_2/CH_4, respectively at 200 °C. Furthermore, outstanding separation factors of 791 and 1946 with a water flux of about 0.5 kg m^{-2} h^{-1} were obtained at 70 °C for the pervaporation of 10 wt% water-containing binary mixtures of methanol and ethanol, respectively. These results unambiguously show that the carbon membranes developed in this work possess the potential for high-temperature hydrogen purification and dewatering of organic solvents.

Published on 01 March 2019. Downloaded by Universiteit Twente on 1/28/2020 1:48:36 PM.

1. Introduction

Membrane technology is recognized as a more energy-efficient alternative for the separation of a wide range of gas and solvent mixtures compared to mature technologies such as pressure swing adsorption and cryogenic distillation. Specific examples include the separation of hydrogen from gasification and hydrocarbons, the upgrading of biogas and landfill gas, flue gas treatment, methane purification and dehydration of organic solvents. In this context, inorganic microporous membranes have been intensively investigated because of thermal and chemical stability issues. The membrane candidates include silica, zeolites, carbon molecular sieve (CMS) and graphene/graphene oxide membranes.

Silica is formed of irregular Si–O–Si rings with an effective size of about 0.3 nm, allowing an efficient separation of smaller size molecules such as H_2O (0.26 nm) and H_2 (0.29 nm). However, its poor stability under hydrothermal conditions limits its application window.[1] Hydrophobic DDR-type zeolites display excellent hydrothermal stability but limited selectivity for smallest gas molecules as they have apertures with an effective size of about 0.4 nm.[2–4] Furthermore, the industrial application of zeolite membranes is hampered by the difficulty in scaling-up due to the formation of inter-crystalline pores or defects. Despite their excellent selectivity, graphene-based membranes[5,6] suffer from insufficient H_2 permeance (10^{-9} to 10^{-8} mol m^{-2} s^{-1} Pa^{-1}) to become technically attractive. Others limitations are associated with high costs required for membrane materials and the complexity in the synthesis procedure of the graphene oxide solution.[7]

Carbon molecular sieve (CMS) membranes, as one of the most promising porous inorganic membranes, have received a growing attention this last decade owing to their unique characteristics such as simple manufacturing and excellent stability under harsh conditions.[8–10] CMS membranes are typically prepared from the pyrolysis/carbonization of various types of polymer precursors in vacuum or inert atmosphere. After decomposition of the thermally unstable polymeric components, a thermally stable carbon backbone consisting of micropores (0.7–2 nm) interconnected with ultra-micropores (<0.7 nm) is formed. In general, the microstructure and the permeation properties of the resulting carbon membrane is significantly affected by the pyrolysis conditions[11–14] (temperature, atmosphere, heating rate and soaking time) and the nature (*i.e.* the chemical structure and morphology) of the polymeric precursor.[15–17] As a result, several CMS membranes have been successfully developed for

[a]Forschungszentrum Jülich GmbH, Institute of Energy and Climate Research, Materials Synthesis and Processing (IEK-1), D-52425 Jülich, Germany. E-mail: p.tchoua@fz-juelich.de

[b]Jülich Aachen Research Alliance: JARA-Energy, Forschungszentrum Jülich GmbH, D-52425 Jülich, Germany

[c]Inorganic Membranes, Faculty of Science and Technology, University of Twente, P. O. Box 217, 7500 AE Enschede, The Netherlands

† Electronic supplementary information (ESI) available. See DOI: 10.1039/c8ta09504c

This journal is © The Royal Society of Chemistry 2019

Published on 01 March 2019. Downloaded by Universiteit Twente on 1/28/2020 1:48:36 PM.

the separation of various important gas and solvents mixtures such as H_2/C_3H_8,[18] CO_2/N_2,[19] CO_2/CH_4 (ref. 14) C_3H_6/C_3H_8 (ref. 20) and H_2O/C_2H_6O.[21]

Nevertheless, it is still challenging to developed ultrathin and defect-free CMS membrane with narrowed pore sizes for efficient separation of H_2–CO_2 gas pairs. As shown in Table 1 most of the supported CMS membranes reported in the literature exhibit H_2/CO_2 selectivities below or slightly above the value, of 4.7, corresponding to the Knudsen diffusion. One of the reasons behind this is attributed to the high porosity and the roughness of the inorganic ceramic support, which leads to the formation of an inhomogeneous polymeric layer that may crack upon pyrolysis. Usually, concentrated polymeric solution or several coating-carbonization cycles are required to minimize the defect formation by improving the membrane thickness. However, this generally compromises the H_2 permeance.[17,22,23] In some cases, intermediate layers such as TiO_2 (ref. 24) and γ-Al_2O_3 (ref. 18) have been successfully introduced to reduce the surface defect of the support and slightly improve the H_2/CO_2 selectivity. However, the obtained separation performances are still unsatisfactory.

Herein, we report on the synthesis and characterization of an ultrathin ($\sim$200 nm) carbon film developed from a polyimide precursor. This work was conducted with the objective of fabricating an ultrathin and defect-free CMS membrane with high H_2/CO_2 selectivity and H_2 permeance at high temperature as a substitute of the hydrothermally unstable silica.

An intermediate γ-Al_2O_3 layer was coated on the inner surface of porous α-Al_2O_3 substrates to facilitate the deposition of a defect-free and ultrathin top layer. A commercially available polyimide resin has been chosen as precursor because of his high glass transition temperature, high carbon content and high quality graphitic microstructure upon carbonization.[11–13] By a careful selection of the pyrolysis conditions, precursor concentration and viscosity, we were able to develop reproducible ultrathin hydrogen-selective CMS membranes with unprecedentedly high separation performance among those for all carbon membranes reported to date. The developed CMS membranes were also tested in the pervaporation dehydration of low molecular weight alcohols such as methanol and ethanol.

2. Experimental

2.1. Precursor and raw materials

Commercial polyimide powder purchased from Alfa Aesar (CAS-number: 62929-02-6) was used as polymer precursor. *N*-Methyl-2-pyrrolidone (NMP) procured by Sigma Aldrich was chosen as the solvent. Tubular α-Al_2O_3 ultrafiltration membranes (length: 300 mm, outer diameter: 10 mm, pore size $\sim$70 nm), sealed at the edges with a glass coating, were obtained from atech innovations GmbH, Germany. α-Al_2O_3 discs with diameter of 39 mm, thickness of 2 mm and pore size of around 80 nm was supplied by Pervatech B.V. Netherlands. Disks-supported membranes were used for characterization tests, while tubular-supported membranes were used for gas permeation and pervaporation tests.

2.2. Membrane preparation

The polymeric solution was prepared by mixing 2 wt% of polyimide powder in NMP and stirring for 10 hours. α-Al_2O_3 discs and tubular α-Al_2O_3 tubes (the inner surface) were dip-coated with a boehmite sol and calcined at 600 °C in air. The coating-calcination procedure was repeated in order to remove large pores that might result in pinholes in the membrane. Upon calcination, γ-Al_2O_3 with mean pore size of around 4 nm (Fig. S1, ESI†) was obtained. The prepared γ-Al_2O_3/α-Al_2O_3 composite supports were then dip-coated with the polymeric solution and dried at 90 °C overnight. An immersion and withdrawal speed of 10 mm s^{-1} with an immersion time of 20 s was applied during the dip-coating process. Note that a horizontal type dip-coater (KSV NIMA) was used for the coating of discs, while a vertical type (Pervatech B.V.) was used for tubular substrates. The dipping-drying process was performed in a class 1000 clean-room in order to avoid dust contamination. The supported polymeric membranes were further placed in the center of a furnace (Gero HTK 25 Mo/16-1G) to undergo heat treatment. A vacuum of about 10^{-6} mbar was applied before starting the carbonization procedure and maintained during the carbonization process. The samples were heated up to 350 °C with heating rate of 1°C min^{-1} and 1 h dwell time at this temperature. The temperature was then subsequently increased

Table 1 H_2 permeance and H_2/CO_2 permselectivities of CMS membranes reported in the literature

Polymeric precursor	Thickness [μm]	Support material	T (°C)	H_2 permeance [mol m^2 s^{-1} Pa^{-1}]	Ideal selectivity	Ref.
Phenolic resin	3.10	α-Al_2O_3	25	1.4×10^{-7}	2.62	19
Phenolic resin	35	Resin	20	1.71×10^{-9}	9.7	22
Phenolic resin	30	Clay/α-Al_2O_3	27	2.7×10^{-8}	14.28	23
Phenolic resin + boehmite	3	α-Al_2O_3	120	5.029×10^{-8}	22.29	25
Phenolic resin + PAA[a]	2	Carbon	25	5.45×10^{-8}	6.2	26
Polyetherimide	4.8	α-Al_2O_3	25	9.07×10^{-8}	3.10	27
Polyetherimide	4	TiO_2/α-Al_2O_3	25	5.3×10^{-8}	8.3	24
Polyimide	1.6	γ-Al_2O_3/α-Al_2O_3	25	$\sim 9 \times 10^{-8}$	3	20
Polyetherimide	2.7	α-Al_2O_3	25	$\sim 1.45 \times 10^{-7}$	2.7	28
Poly(amid acid)	$\sim$100	Carbon	30	6.84×10^{-9}	9.5	17
Polyester	0.125	γ-Al_2O_3/α-Al_2O_3	150	$\sim 6.3 \times 10^{-7}$	$\sim$8	18

[a] PAA: poly(amid acid); 1 barrer = 10^{-10} cm^3 (STP) cm/cm^2 s cmHg.

Published on 01 March 2019. Downloaded by Universiteit Twente on 1/28/2020 1:48:36 PM.

to 700 °C using the same heating rate and samples treated for further 2 hours. The membranes were cooled down to room temperature using a cooling rate of 1°C min^{-1}.

2.3. Membrane characterization

Several techniques including Fourier transform infrared spectroscopy (FTIR), X-ray photoelectron spectroscopy (XPS), water contact angle and scanning electron microscopy have been employed.

The chemical structure of both membranes was determined using and Infrared spectrometer "Tensor 27" (Bruker Optics) equipped with a DTGS detector and a Golden Gate diamond attenuated total reflectance (ATR) unit containing ZnSe mirrors. The resolution of the spectrometer was set at 4 cm^{-1}. All spectra were collected in the range of 600–4000 cm^{-1} and normalized to the gradient vector for comparison.

XPS measurements were performed using a PHI5000 Versa Probe II from ULVAC-PHI Inc., USA. Core level spectra (C1s, O1s, C1s and N1s) of the supported membranes were recorded with an Al k-alpha (1.486 keV) source for excitation in the analysis chamber under high vacuum (1×10^{-8} mbar) and at pass energy of 23.5 eV with a resolution of 0.1 eV. The atomic ratios and surface concentrations were quantitatively determined from the area of the C1s, N1s and O1s peaks after a smart-type background subtraction, while the peak deconvolution was achieved using a mixed Gaussian and Lorentzian function. The binding energy was normalized by setting the C1s core level to 285 eV (sp^3) and 284.5 eV (sp^2).

Water contact angle measurements were performed at room temperature by the sessile drop method using a contact angle goniometer, equipped with video camera recording system, and using software for drop-shape analysis. The water droplet with a volume of 3 μl was placed at four different regions of the dip-coated membranes surface. For each, the contact angle was measured and the average value was taken. The surface morphology and the thickness of the supported membranes were investigated by using a scanning electron microscope (SEM Ultra 55, Carl Zeiss Microscopy GmbH, Jena, Germany). Cross-section images were obtained by fracture using a pair of cutting pliers. The samples were coated with a conductive layer prior analysis.

2.4. Gas permeation test

The single gas permeation of H_2, CO_2, N_2 and CH_4 was measured using an in-house made dead-end mode permeation test rig with a stainless steel tubular membrane module. The permeate stream was kept at atmospheric pressure, and the pressure through the membrane was maintained at 2 bar. The gas flow at the feed side of the module was controlled by an accurate pressure controller (Bronkhorst differential, pressure controller with a F-001 valve). The gas flow rate at the permeate side was measured using two flow meters with maximum flow of 7.74 ml min^{-1} and 209 ml min^{-1} (Brooks GF40). Before evaluation of the permeation properties, the membranes were dried at 200 °C overnight in vacuum. Gas permeance and ideal selectivity were calculated using eqn (1) and (2), respectively.

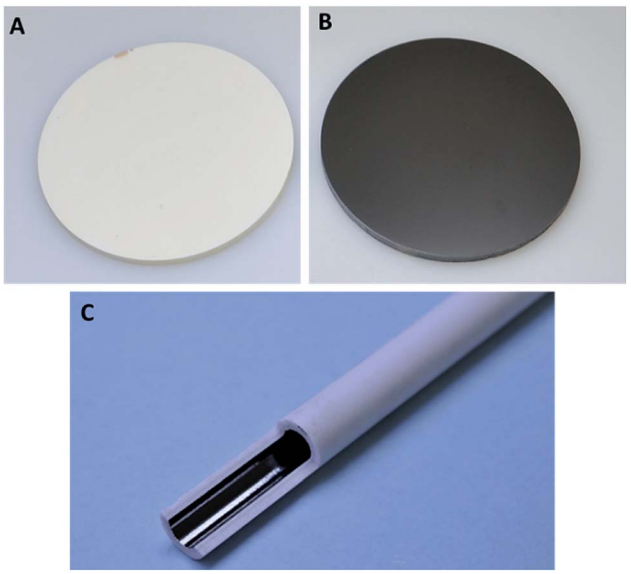

Fig. 1 Photographs of the α-Al_2O_3/γ-Al_2O_3-supported polyimide membrane before (A) and after (B and C) the pyrolysis at 700 °C.

$$P_i = \frac{F_i}{A \times \Delta P_i} \quad (1)$$

$$\alpha_{ij} = \frac{P_i}{P_j} \quad (2)$$

where P_i and P_j [mol m^{-2} s^{-1} Pa^{-1}] are the permeance of components i and j respectively, F_i [mol s^{-1}] represents the flow rate of the component i, A [m^2] is the effective membrane area, ΔP_i [Pa] the partial pressure of component i between the feed and the permeate side of the tubular membrane, and α_{ij} is the permeance ratio of component i over j. Gas permeance was measured from 200 °C to 50 °C and a test series of 3 samples was performed for each membrane with a good reproducibility of gas permeance.

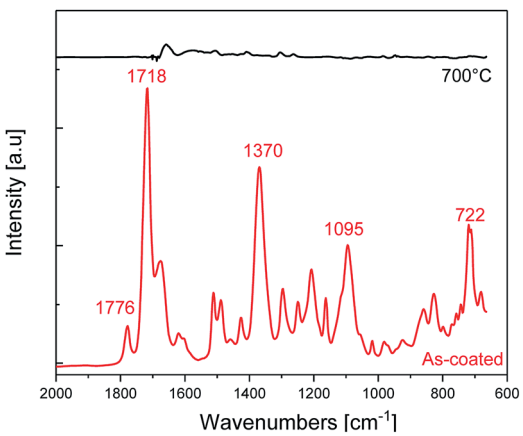

Fig. 2 ATR-FTIR spectra of the α-Al_2O_3/γ-Al_2O_3-supported polyimide membrane before (red line) and after (black line) the pyrolysis at 700 °C.

This journal is © The Royal Society of Chemistry 2019

Published on 01 March 2019. Downloaded by Universiteit Twente on 1/28/2020 1:48:36 PM.

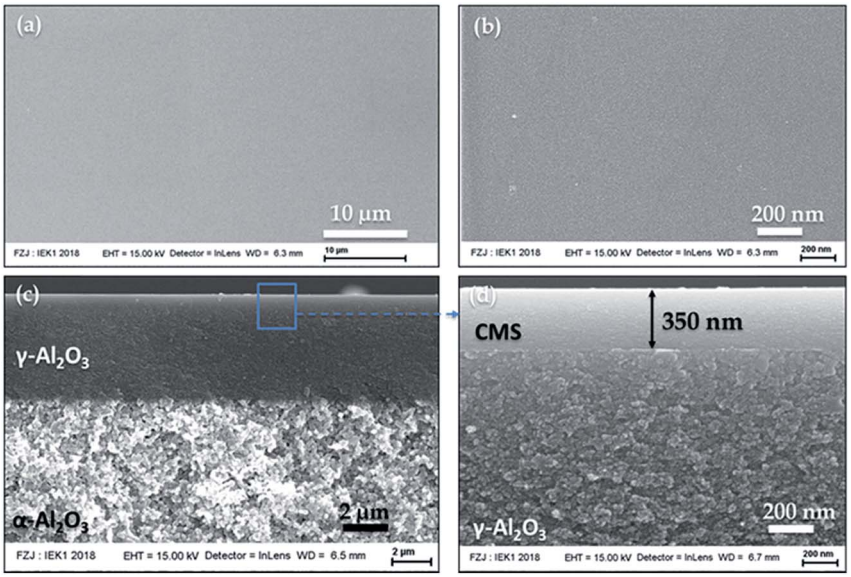

Fig. 3 SEM images of the top surface (a and b) and of the cross-section (c and d) of the α-Al_2O_3/γ-Al_2O_3-supported planar CMS membrane.

2.5. Pervaporation test

A commercial cross-flow test unit (Pervatech B.V. Netherlands) was used for the evaluation of the pervaporation performance of tubular CMS membranes. Briefly, the feed, containing 10 wt% in alcohol (methanol or ethanol) was heated at 70 °C. The CMS membrane side faces the feed side (feed flow: 300 l h^{-1} and feed volume 2 L), while the permeate side was kept was at a pressure of 10 mbar by means of a vacuum pump. The water concentrations in the feed and permeate were determined by Karl-Fischer titrations and the refractive index (Mettler Toledo RA510M) under ambient conditions, respectively. The permeate stream was collected in a vacuum trap using liquid nitrogen. The permeation flux J and the separation factor α_{ij} is calculated using eqn (3) and (4), respectively

$$J = \frac{Q}{A \times t} \quad (3)$$

$$\alpha_{ij} = \frac{Y_i \times X_j}{X_i \times Y_j} \quad (4)$$

where J [g] is the weight of the collected permeate during the experimental time t [h], A [m^2] is the effective membrane area surface, X and Y represent the mole fraction of component i and j in the feed and permeate, respectively. The pervaporation results are obtained after 1 day of continuous operation, allowing a more precise comparison of fluxes and selectivities.

3. Results and discussions

3.1. Membrane characterization

Fig. 1a–c displays the photographs of the α-Al_2O_3/γ-Al_2O_3-supported polyimide membrane before and after the heat treatment at 700 °C in vacuum. A homogeneous yellow coating can be seen after dipping the composite support into the polyimide solution. The color of the coating changes from yellow to black color upon annealing at 700 °C, indicating a pyrolysis process.

Fig. 2 shows the ATR-FTIR spectra of the supported membranes before and after heat treatment. The supported polymeric membrane is characterized by the appearance of the peaks at 1776 cm^{-1} (C═O asymmetric stretching), 1720 cm^{-1} (C═O symmetric stretching), 1370 cm^{-1} and 1095 (OC–N–CO stretching) and 722 cm^{-1} (C–N–C bending), which correspond to the characteristic absorption of the imide group.[29,30] The intensity of these peaks drastically degrades upon treating the samples at 700 °C. This suggests that the degradation of the polymer is dictates by the transformation of the imide groups.[31]

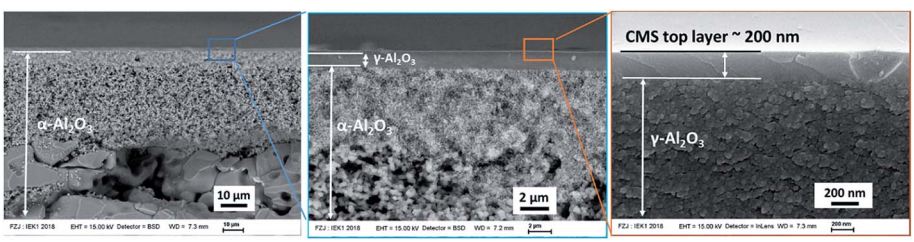

Fig. 4 Cross-sectional SEM images of the α-Al_2O_3/γ-Al_2O_3-supported tubular CMS membrane.

Published on 01 March 2019. Downloaded by Universiteit Twente on 1/28/2020 1:48:36 PM.

The surface morphology and the thickness of the CMS top layer are investigated by means scanning electron microscopy as shown Fig. 3 and 4.

A dense, uniform, smooth and crack-free carbon layer is formed with a good adhesion to the γ-Al_2O_3 interlayer. The tubular alpha alumina substrate exhibits an asymmetric structure with a graded porosity. The thickness of the CMS top layer was found to be approximately 350 nm and 200 nm for planar and tubular membranes, respectively. The difference in thickness can be explained by the difference in coating technique as report in the experimental part.

The surface elemental composition of the polymeric and CMS membrane, determined by XPS, is presented in Table 2. The oxygen-to-carbon ratio decreases from 18.3% to 7.6% after pyrolysis. Furthermore, 7 at% and 1.9 at% of oxygen and nitrogen are respectively detected at the surface of the carbonized sample. This suggests the presence of oxygen and nitrogen-containing functional groups. In order to get more insights into the structural changes (electronic environments and bonding structures) induced by the heat treatment, C1s XPS spectra of the polymeric and carbonized samples were deconvoluted using a model based on a set of Gaussian–lorentzian functions as shown in Fig. 5 the supported polyimide membrane shows of three contributions centered at 285.0, 286.0 and 288.5 eV, which correspond to the C–C (sp^3) bond of an aromatic ring not attached to imide rings, C–N and C═O bonds within imide rings, respectively.[32,33] The C–N bonding is also confirmed by a single broad peak at around 400.3 eV from N1s core-level spectra[32,33] (Fig S2 ESI†). Three peaks are found in the O1s spectrum (Fig. S3 ESI†) which represent C═O (531.3 eV), C–O (532.5 eV) and O–H (533.8 eV), respectively.[32,33] The presence of graphitic carbon after pyrolysis is indicated in the C1s spectrum (Fig. 5) by the occurrence of a peak at 284.5 eV (58 at%), corresponding to C═C bonding within a sp^2 network.[32,33] The presence of non-graphitic carbon is attested by the peak at 285.0 eV, corresponding to C–C bond (sp^3) and a broad peak at 286 eV, which can be ascribed to nitrogen and oxygen containing functional groups such as C–N, C═N, C≡N, and C–O.[32,33] Note that the presence of these functional groups after the heat treatment is also confirmed by the deconvolution of the N1s (Fig S2 ESI†) and O1s (Fig S3 ESI†) spectra, respectively. Based on the XPS analysis, the carbon membrane developed in this work is a mixture of graphitic and amorphous carbon. The latter represents "defects" within or at the edge of the graphitic layers.

Table 2 Surface elemental composition of the α-Al_2O_3/γ-Al_2O_3-supported polyimide membrane prior and after the heat treatment at 700 °C

	XPS analysis (at%)			
Membrane	C1s	O1s	N1s	O/C ratio
As-coated	80.8	14.8	4.4	18.3
700 °C	91.1	7.0	1.9	7.6

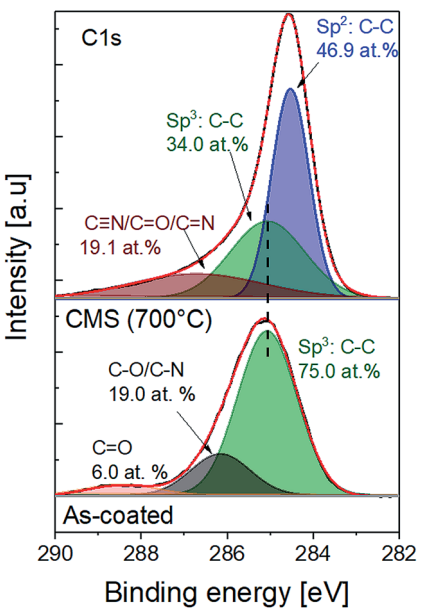

Fig. 5 C1s XPS spectra of the α-Al_2O_3/γ-Al_2O_3-supported polyimide membrane before (bottom graph) and after the heat treatment at 700 °C (top graph).

The nature or type of defects in the graphitic layers of the CMS membrane is probed by means of Raman spectroscopy. As shown in Fig. 6, the Raman spectrum of the carbonized sample is fitted by means of five Gaussian contributions.[33,34] The peak centered at 1600 cm^{-1} is defined as G band and is attributed to the in-plane stretching mode of E_{2g} symmetry at sp^2 sites. This band is solely observed in perfect infinite graphitic planes as for single crystal graphite. When defects are present within the graphene planes, the D1 band becomes Raman active because of the activation of the breathing mode of carbon rings of A_{1g} symmetry at the edge of graphite planes. The D2 at 1635 cm^{-1} peak is associated with lattice vibrations as for D1 but involving isolated graphene layers. D3 and D4 bands generally appear for highly defectives carbonaceous materials. The former at 1560 cm^{-1} is usually broad and is ascribed to amorphous carbon, while the latter at 1150 cm^{-1} is attributed to sp^3 impurities. By means of Raman spectroscopy, Eckmann *et al.*[35] used the intensity ratio of D1 and D2 peaks

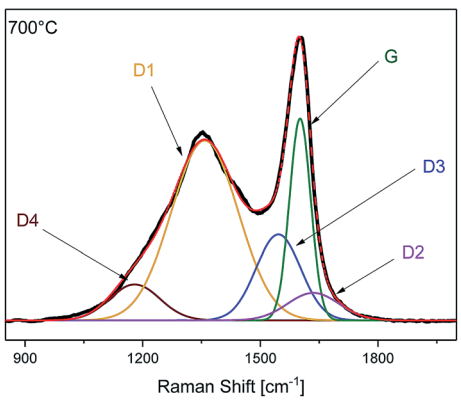

Fig. 6 Raman spectrum of the α-Al_2O_3/γ-Al_2O_3-supported CMS membrane.

This journal is © The Royal Society of Chemistry 2019

Published on 01 March 2019. Downloaded by Universiteit Twente on 1/28/2020 1:48:36 PM.

(I_{D1}/I_{D2}) to probe the type of defects in graphene samples, which were introduced by fluorination (sp^3-type defects) and Ar^+-bombardment (vacancy-like defects). They found an I_{D1}/I_{D2} ratio of about 13 for defects associated with sp^3 hybridization and 7 for vacancy like-defects. In this work, the calculated I_{D1}/I_{D2} intensity ratio is found to be about 13.15, indicating that most of defects in our carbonized sample are sp^3 type-defects. This result is in agreement with XPS analysis which has shown that 34 at% of the total amount of carbon is associated with sp^3 hybridization.

3.2. Gas separation performance

The gas separation performance of tubular CMS membranes is evaluated by measuring the permeance of several gases with different kinetic diameters at 200 °C and at a feed pressure of difference of 2 bar. Three membranes from different every batch were tested to guarantee the reliability of the results (Fig. S4 and Table S1, ESI†). As shown in Fig. 7, the permeance values of the selected gases increases with decreasing kinetic diameter *i.e.* CH_4 (0.38 nm) > N_2 (0.365 nm) > CO_2 (0.33 nm) > H_2 (0.29 nm). This suggests that the transport of these gases through the CMS membrane is governed by the molecular sieving mechanism. Important information on the gas transport behavior can be obtained by measuring the temperature dependence of gas permeances through the CMS membrane. As shown in Fig. 8A, the permeation of all gases increases with the temperature. For instance, H_2 shows the highest permeance, which increases for almost one order of magnitude in the range of 50 to 200 °C. The perm-selectivity of all gas pairs also increases with increasing the temperature (Fig. 8B). At 200 °C, the CMS membrane exhibits perm-selectivities of about 24, 130 and 228 for H_2/CO_2, H_2/N_2 and H_2/CH_4 gas pairs, respectively, which by far exceed the corresponding Knudsen coefficients (4.7, 3.7 and 2.8). Such excellent permselectivities demonstrates the pinhole-free nature of the developed CMS membranes and are attributed to the presence of ultra-micropores, which prevent the diffusion of larger gas molecules such as N_2 and CH_4. Therefore, we can assume that the pore size of our CMS membrane is close to the kinetic diameter of CO_2 *i.e.* 0.33 nm.

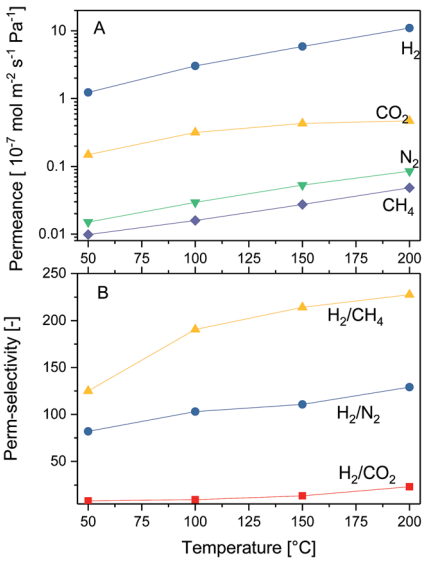

Fig. 8 Temperature dependence of the single gas permeance (A) and perm-selectivity (B) for the α-Al_2O_3/γ-Al_2O_3-supported CMS membrane at 2 bar feed pressure.

The apparent activation energy, E_{act}, for the permeation of H_2, CO_2, N_2 and CH_4 through the CMS membrane is calculated from the Arrhenius temperature dependence of the permeation.

Excellent linear fits were obtained for all samples with the resultant E_{act} indicated in Fig. S5 (ESI†). The highest E_{act} value, 17.8 kJ mol^{-1}, is obtained for H_2, while the lowest value, of 9.9 kJ mol^{-1}, corresponds to the permeation of CO_2. This means that the CMS membrane can exhibit excellent H_2/CO_2 separation performance at elevated temperature. It should be noted that the E_{act} for H_2 obtained in this work is comparable with those reported for silica[36] and graphene[5] membranes.

The excellent gas separation performance exhibited by our CMS membrane at 200 °C can be attributed to several

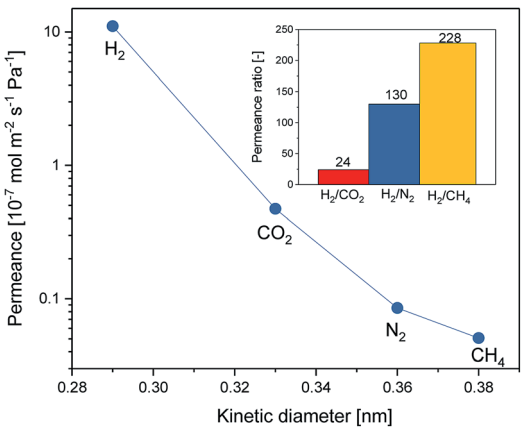

Fig. 7 Single gas permeation through the α-Al_2O_3/γ-Al_2O_3-supported CMS membrane with a feed pressure of 2 bar at 200 °C. The inset displays the ideal separation factors.

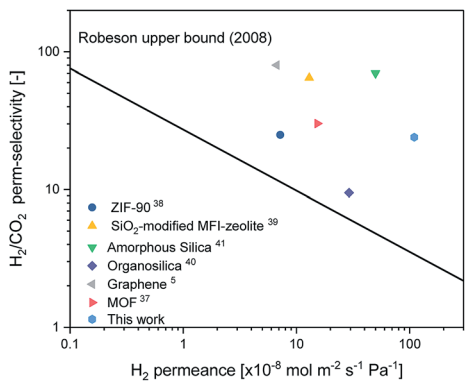

Fig. 9 Comparison of the H_2/CO_2 separation performance of the α-Al_2O_3/γ-Al_2O_3-supported CMS membrane with the-state-of-the-art-microporous inorganic membranes in the temperature range of 150–200 °C. The solid black line represents the polymer upper bound.

Published on 01 March 2019. Downloaded by Universiteit Twente on 1/28/2020 1:48:36 PM.

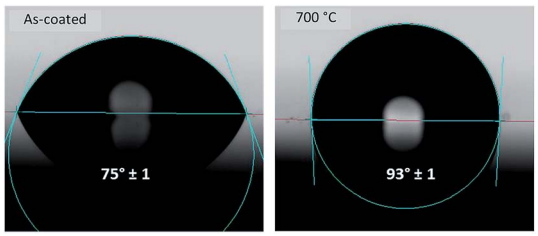

Fig. 10 Representative shapes of water droplets on the α-Al_2O_3/γ-Al_2O_3-supported polyimide-membrane prior (left panel) and after (right panel) the heat treatment.

parameters such as the membrane configuration, the choice of the polymeric precursor and the pyrolysis conditions. In fact, the presence of the mesoporous γ-Al_2O_3 layer enables the synthesis and deposition of a high-quality polyimide thin film and the subsequent formation of a thin and pinhole-free carbon selective layer. The H_2/CO_2 separation performance of our carbon membrane is further compared with other state-of-the-art materials, including MOF,[37] ZIF,[38] silica modified zeolite,[39] silica[40,41] and graphene[5] (Fig. 9). The solid line represents the Robeson upper bound tradeoff between H_2 permeance and H_2/CO_2 selectivity for polymeric membrane, assuming a membrane thickness of 50 μm.[42] The H_2/CO_2 selectivity of our carbon membrane is well above the tradeoff curve and is only surpassed by those of amorphous silica, silica-modified MFI zeolite and graphene. However, all these membranes display a relatively low H_2 permeance than our CMS membrane. For instance, the graphene membrane developed by van Gestel *et al.*[5] exhibits the largest H_2/CO_2 permselectivity (about 80) because of the perfect layered structure of the graphene planes, restricting the diffusion of CO_2. Nevertheless, the H_2 permeance, 6.7×10^{-8} mol m^{-2} s^{-1} Pa^{-1}, is more than one order of magnitude lower than that, 1.1×10^{-6} mol m^{-2} s^{-1} Pa^{-1}, of the carbon membrane developed in the present work. The enhanced H_2 permeance of our carbon membrane can be attributed to the presence of sp^3-type defects in the graphene planes, enabling the faster diffusion of H_2.

Considering these results, we can conclude that this carbon membrane displays both high H_2/CO_2 selectivity and high H_2 permeance, which are important performance parameters for an industrial application.

3.3. Pervaporation performance

The surface wettability of the membrane surface with respect to water can be easily estimated by measuring the water contact angle. The water angle of the polymeric membrane prior and after the heat treatment is shown in Fig. 10. The pristine membrane displays a contact angle of about 75°, which increase to about 90° after thermal treatment. This is attributed to the increase of the carbon content, making the membrane more hydrophobic. It should be noted that water contact angles in the range of 95–100° have been reported for graphene.[43,44] The lower contact angle measured for our CMS membrane compared to that of graphene can be partially ascribed to the presence of some oxygen-containing functional groups (7 at%) at the membrane surface, as mentioned in Section 3.1.

Table 3 summarizes the pervaporation results for 10 wt% water-containing binary liquid feeds through the CMS membrane at 70 °C. Methanol and ethanol were used as feed solutions because of their difference in molecular sizes. The pervaporation results are obtained after 1 day of continuous operation, allowing a more precise comparison of fluxes and selectivities. It can be seen from Table 3 that the separation factor increases with the molecular size of the alcohol. This confirms the excellent molecular sieving ability of the developed carbon membranes.

Table 4 compares the pervaporation performance for methanol dehydration of the carbon membrane developed in this

Table 3 Pervaporation results of H_2O/alcohol (10/90 wt%) through the α-Al_2O_3/γ-Al_2O_3-supported CMS membrane at 70 °C

Alcohol	Molecular size [nm]	H_2O permeate (w/w%)	J_{H_2O} (g m^{-2} h^{-1})	$J_{Alcohol}$ (g m^{-2} h^{-1})	$\alpha_{H_2O/Alcohol}$
Methanol	0.38	99.0	527.5	5.3	791
Ethanol	0.42	99.5	541.8	2.7	1946

Table 4 Comparison of pervaporation membranes applied to aqueous methanol dehydration

Membrane	Feed H_2O (wt%)	T (°C)	J_{total} (kg m^{-2} h^{-1})	α	PSI[c] (kg m^{-2} h^{-1})	Ref.
Carbon[a], tubular	10	50	0.13	65	8	49
Carbon[b] hollow fiber	10	60	0.32	11	3	50
Silica (Pervatech), tubular	15	50	0.70	7	4	48
Silica (ECN), tubular	10	90	2.20	55	119	47
Silica, tubular	2	60	0.06	200	12	46
NaA-zeolite, tubular	70	60	1.8	140	250	45
Carbon, tubular	10	70	0.529	791	418	This work

[a] Resorcinol. [b] Poly(phenylene oxide). [c] PSI = $J_{total} \times (\alpha - 1)$.

This journal is © The Royal Society of Chemistry 2019

Published on 01 March 2019. Downloaded by Universiteit Twente on 1/28/2020 1:48:36 PM.

work with NaA zeolite,[45] silica[46–48] and carbon[49,50] membranes. The pervaporation index (PSI) is used as an indicator of the performance of the synthesized membrane.[51] Our CMS membrane displays a lower water flux compare to the hydrophilic membranes including NaA type zeolite and silica membranes, but the highest separation factor and PSI. This means that despite its hydrophobic character, this CMS membrane can effectively separate water from aqueous alcohol mixtures based on molecular sieve mechanism.

4. Conclusions

Thin and pinhole-free carbon molecular sieve membranes were reproducibly prepared by carbonization of a commercial polyimide resin at 700 °C on composite α-Al_2O_3/γ-Al_2O_3 supports. XPS and Raman characterizations have shown that the pyrolyzed carbon membrane is a mixture of amorphous and "turbostratic" carbon. Single gas permeation measurements showed that the membrane reproducibly delivered a H_2 permeance in the range of 1×10^{-6} mol m^{-2} s^{-1} Pa^{-1} with permselectivities of H_2 over CO_2, N_2 and CH_4 of about 24, 130 and 228, respectively at 200 °C. Which values are the highest separation performances reported for carbon membranes. These outstanding results were ascribed to the excellent molecular sieve character of these membranes, showing a stronger temperature dependency for the permeation of small-size gas (H_2) than large-size gases (CO_2, N_2 and CH_4). The developed carbon membranes also exhibit unprecedented separation performance towards the dehydration of aqueous alcohol mixtures, even for the more challenging water–methanol mixture. Based on our results, it can be concluded that the membranes developed in this work have great potential in high-temperature hydrogen purification and dewatering of aqueous alcohol mixtures.

Conflicts of interest

There are no conflicts to declare.

Acknowledgements

The German Federal Ministry for Economic Affairs and Energy (BMWi) is greatly acknowledged for its financial support to the MemKoR project within the COORETEC program under the grant number: 03ET7064B. Mrs Hiltrud Moitroux (digital photographs); Mr Lars Petter (Gas permeation tests); Dr Doris Sebold (FE-SEM images); Dr Sandra Lobe (Raman measurements); Dr Astrid Besmehn (ATR-FTIR measurements); Dr Heinrich Hartmann (XPS measurements) and Pervatech B.V. (Pervaporation tests) are also acknowledged.

References

1 T. Nagano and K. Sato, Degradation mechanism of an H-2-permselective amorphous silica membrane, *J. Mater. Sci.*, 2014, **49**(11), 4115–4120.
2 S. Himeno, T. Tomita, K. Suzuki, K. Nakayama, K. Yajima and S. Yoshida, Synthesis and permeation properties of a DDR-type zeolite membrane for separation of CO_2/CH_4 gaseous mixtures, *Ind. Eng. Chem. Res.*, 2007, **46**(21), 6989–6997.
3 T. Tomita, K. Nakayama and H. Sakai, Gas separation characteristics of DDR type zeolite membrane, *Microporous Mesoporous Mater.*, 2004, **68**(1–3), 71–75.
4 S. W. Yang, Z. S. Cao, A. Arvanitis, X. H. Sun, Z. Xu and J. H. Dong, DDR-type zeolite membrane synthesis, modification and gas permeation studies, *J. Membr. Sci.*, 2016, **505**, 194–204.
5 T. Van Gestel and J. Barthel, New types of graphene-based membranes with molecular sieve properties for He, H-2 and H_2O, *J. Membr. Sci.*, 2018, **554**, 378–384.
6 A. Ibrahim and Y. S. Lin, Gas permeation and separation properties of large-sheet stacked graphene oxide membranes, *J. Membr. Sci.*, 2018, **550**, 238–245.
7 N. I. Zaaba, K. L. Foo, U. Hashim, S. J. Tan, W. W. Liu and C. H. Voon, Synthesis of Graphene Oxide using Modified Hummers Method: Solvent Influence, in *Advances in Material & Processing Technologies Conference*, ed. I. A. Choudhury, H. S. C. Metselaar and N. BinYusoff, 2017, pp. 469–477.
8 M. Abdollahi, J. Yu, P. K. T. Liu, R. Ciora, M. Sahimi and T. T. Tsotsis, Hydrogen production from coal-derived syngas using a catalytic membrane reactor based process, *J. Membr. Sci.*, 2010, **363**(1–2), 160–169.
9 P. K. T. Liu, M. Sahimi and T. T. Tsotsis, Process intensification in hydrogen production from coal and biomass *via* the use of membrane-based reactive separations, *Curr. Opin. Chem. Eng.*, 2012, **1**(3), 342–351.
10 D. Parsley, R. J. Ciora, D. L. Flowers, J. Laukaitaus, A. Chen, P. K. T. Liu, J. Yu, M. Sahimi, A. Bonsu and T. T. Tsotsis, Field evaluation of carbon molecular sieve membranes for the separation and purification of hydrogen from coal- and biomass-derived syngas, *J. Membr. Sci.*, 2014, **450**, 81–92.
11 V. C. Geiszler and W. J. Koros, Effects of polyimide pyrolysis conditions on carbon molecular sieve membrane properties, *Ind. Eng. Chem. Res.*, 1996, **35**(9), 2999–3003.
12 K. M. Steel and W. J. Koros, An investigation of the effects of pyrolysis parameters on gas separation properties of carbon materials, *Carbon*, 2005, **43**(9), 1843–1856.
13 K. M. Steel and W. J. Koros, Investigation of porosity of carbon materials and related effects on gas separation properties, *Carbon*, 2003, **41**(2), 253–266.
14 N. Sazali, W. N. W. Salleh, N. Nordin and A. F. Ismail, Matrimid-based carbon tubular membrane: effect of carbonization environment, *J. Ind. Eng. Chem.*, 2015, **32**, 167–171.
15 Y. C. Xiao, T. S. Chung, M. L. Chng, S. Tarnai and A. Yamaguchi, Structure and properties relationships for aromatic polyimides and their derived carbon membranes: Experimental and simulation approaches, *J. Phys. Chem. B*, 2005, **109**(40), 18741–18748.
16 P. S. Tin, Y. C. Xiao and T. S. Chung, Polyimide-carbonized membranes for gas separation: Structural, composition,

Published on 01 March 2019. Downloaded by Universiteit Twente on 1/28/2020 1:48:36 PM.

and morphological control of precursors, *Sep. Purif. Rev.*, 2006, **35**(4), 285–318.

17 H. B. Park, Y. K. Kim, J. M. Lee, S. Y. Lee and Y. M. Lee, Relationship between chemical structure of aromatic polyimides and gas permeation properties of their carbon molecular sieve membranes, *J. Membr. Sci.*, 2004, **229**(1–2), 117–127.

18 H. Richter, H. Voss, N. Kaltenborn, S. Kamnitz, A. Wollbrink, A. Feldhoff, J. Caro, S. Roitsch and I. Voigt, High-Flux Carbon Molecular Sieve Membranes for Gas Separation, *Angew. Chem., Int. Ed.*, 2017, **56**(27), 7760–7763.

19 M. A. L. Tanco, D. A. P. Tanaka, S. C. Rodrigues, M. Texeira and A. Mendes, Composite-alumina-carbon molecular sieve membranes prepared from novolac resin and boehmite. Part I: preparation, characterization and gas permeation studies, *Int. J. Hydrogen Energy*, 2015, **40**(16), 5653–5663.

20 X. L. Ma, B. K. Lin, X. T. Wei, J. Kniep and Y. S. Lin, Gamma-Alumina Supported Carbon Molecular Sieve Membrane for Propylene/Propane Separation, *Ind. Eng. Chem. Res.*, 2013, **52**(11), 4297–4305.

21 K. S. Liao, Y. J. Fu, C. C. Hu, J. T. Chen, D. W. Lin, K. R. Lee, K. L. Tung, Y. C. Jean and J. Y. Lai, Microstructure of carbon molecular sieve membranes and their application to separation of aqueous bioethanol, *Carbon*, 2012, **50**(11), 4220–4227.

22 W. Wei, G. T. Qin, H. Q. Hu, L. B. You and G. H. Chen, Preparation of supported carbon molecular sieve membrane from novolac phenol-formaldehyde resin, *J. Membr. Sci.*, 2007, **303**(1–2), 80–85.

23 S. Roy, R. Das, M. K. Gagrai and S. Sarkar, Preparation of carbon molecular sieve membrane derived from phenolic resin over macroporous clay-alumina based support for hydrogen separation, *J. Porous Mater.*, 2016, **23**(6), 1653–1662.

24 H. H. Tseng, C. T. Wang, G. L. Zhuang, P. Uchytil, J. Reznickova and K. Setnickova, Enhanced H-2/CH_4 and H-2/CO_2 separation by carbon molecular sieve membrane coated on titania modified alumina support: effects of TiO_2 intermediate layer preparation variables on interfacial adhesion (vol 510, pg 391, 2016), *J. Membr. Sci.*, 2018, **554**, 274.

25 S. C. Rodrigues, R. Whitley and A. Mendes, Preparation and characterization of carbon molecular sieve membranes based on resorcinol-formaldehyde resin, *J. Membr. Sci.*, 2014, **459**, 207–216.

26 L. Li, C. W. Song, H. W. Jiang, J. S. Qiu and T. H. Wang, Preparation and gas separation performance of supported carbon membranes with ordered mesoporous carbon interlayer, *J. Membr. Sci.*, 2014, **450**, 469–477.

27 M. Y. Wey, H. H. Tseng and C. K. Chiang, Improving the mechanical strength and gas separation performance of CMS membranes by simply sintering treatment of alpha-Al_2O_3 support, *J. Membr. Sci.*, 2014, **453**, 603–613.

28 H. H. Tseng, K. M. Shih, P. T. Shiu and M. Y. Wey, Influence of support structure on the permeation behavior of polyetherimide-derived carbon molecular sieve composite membrane, *J. Membr. Sci.*, 2012, **405**, 250–260.

29 S. Kim, K. S. Jang, H. D. Choi, S. H. Choi, S. J. Kwon, I. D. Kim, J. A. Lim and J. M. Hong, Porous Polyimide Membranes Prepared by Wet Phase Inversion for Use in Low Dielectric Applications, *Int. J. Mol. Sci.*, 2013, **14**(5), 8698–8707.

30 D. Guzman-Lucero, J. F. Palomeque-Santiago, C. Camacho-Zuniga, F. A. Ruiz-Trevino, J. Guzman, A. Galicia-Aguilar and C. Aguilar-Lugo, Gas Permeation Properties of Soluble Aromatic Polyimides Based on 4-Fluoro-4,4'-Diaminotriphenylmethane, *Materials*, 2015, **8**(4), 1951–1965.

31 H. Hatori, Y. Yamada, M. Shiraishi, M. Yoshihara and T. Kimura, The mechanism of polyimide pyrolysis in the early stage, *Carbon*, 1996, **34**(2), 201–208.

32 P. Murugaraj, D. E. Mainwaring, M. Al Kobaisi and R. Siegele, Stable doped sp(2) C-hybrid nanostructures by reactive ion beam irradiation, *J. Mater. Chem.*, 2012, **22**(35), 18403–18410.

33 P. Parent, C. Laffon, I. Marhaba, D. Ferry, T. Z. Regier, I. K. Ortega, B. Chazallon, Y. Carpentier and C. Focsa, Nanoscale characterization of aircraft soot: a high-resolution transmission electron microscopy, Raman spectroscopy, X-ray photoelectron and near-edge X-ray absorption spectroscopy study, *Carbon*, 2016, **101**, 86–100.

34 H. J. Seong and A. L. Boehman, Evaluation of Raman Parameters Using Visible Raman Microscopy for Soot Oxidative Reactivity, *Energy Fuels*, 2013, **27**(3), 1613–1624.

35 A. Eckmann, A. Felten, A. Mishchenko, L. Britnell, R. Krupke, K. S. Novoselov and C. Casiraghi, Probing the Nature of Defects in Graphene by Raman Spectroscopy, *Nano Lett.*, 2012, **12**(8), 3925–3930.

36 C. Yacou, S. Smart and J. C. D. da Costa, Long term performance cobalt oxide silica membrane module for high temperature H-2 separation, *Energy Environ. Sci.*, 2012, **5**(2), 5820–5832.

37 Z. X. Kang, M. Xue, L. L. Fan, L. Huang, L. J. Guo, G. Y. Wei, B. L. Chen and S. L. Qiu, Highly selective sieving of small gas molecules by using an ultra-microporous metal-organic framework membrane, *Energy Environ. Sci.*, 2014, **7**(12), 4053–4060.

38 A. S. Huang, W. Dou and J. Caro, Steam-Stable Zeolitic Imidazolate Framework ZIF-90 Membrane with Hydrogen Selectivity through Covalent Functionalization, *J. Am. Chem. Soc.*, 2010, **132**(44), 15562–15564.

39 Z. Tang, J. H. Dong and T. M. Nenoff, Internal Surface Modification of MFI-Type Zeolite Membranes for High Selectivity and High Flux for Hydrogen, *Langmuir*, 2009, **25**(9), 4848–4852.

40 H. T. Song, Y. B. Wei and H. Qi, Tailoring pore structures to improve the permselectivity of organosilica membranes by tuning calcination parameters, *J. Mater. Chem. A*, 2017, **5**(47), 24657–24666.

41 R. M. de Vos and H. Verweij, High-selectivity, high-flux silica membranes for gas separation, *Science*, 1998, **279**(5357), 1710–1711.

42 H. Li, Z. N. Song, X. J. Zhang, Y. Huang, S. G. Li, Y. T. Mao, H. J. Ploehn, Y. Bao and M. Yu, Ultrathin, Molecular-Sieving

 This journal is © The Royal Society of Chemistry 2019

Published on 01 March 2019. Downloaded by Universiteit Twente on 1/28/2020 1:48:36 PM.

Graphene Oxide Membranes for Selective Hydrogen Separation, *Science*, 2013, **342**(6154), 95–98.

43 Z. T. Li, Y. J. Wang, A. Kozbial, G. Shenoy, F. Zhou, R. McGinley, P. Ireland, B. Morganstein, A. Kunkel, S. P. Surwade, L. Li and H. T. Liu, Effect of airborne contaminants on the wettability of supported graphene and graphite, *Nat. Mater.*, 2013, **12**(10), 925–931.

44 F. Taherian, V. Marcon, N. F. A. van der Vegt and F. Leroy, What Is the Contact Angle of Water on Graphene?, *Langmuir*, 2013, **29**(5), 1457–1465.

45 D. Shah, K. Kissick, A. Ghorpade, R. Hannah and D. Bhattacharyya, Pervaporation of alcohol-water and dimethylformamide-water mixtures using hydrophilic zeolite NaA membranes: mechanisms and experimental results, *J. Membr. Sci.*, 2000, **179**(1–2), 185–205.

46 R. W. Vangemert and F. P. Cuperus, Newly Developed Ceramic Membranes for Dehydration and Separation of Organic Mixtures by Pervaporation, *J. Membr. Sci.*, 1995, **105**(3), 287–291.

47 S. Sommer and T. Melin, Influence of operation parameters on the separation of mixtures by pervaporation and vapor permeation with inorganic membranes. Part 1: dehydration of solvents, *Chem. Eng. Sci.*, 2005, **60**(16), 4509–4523.

48 J. E. ten Elshof, C. R. Abadal, J. Sekulic, S. R. Chowdhury and D. H. A. Blank, Transport mechanisms of water and organic solvents through microporous silica in the pervaporation of binary liquids, *Microporous Mesoporous Mater.*, 2003, **65**(2–3), 197–208.

49 S. Tanaka, T. Yasuda, Y. Katayama and Y. Miyake, Pervaporation dehydration performance of microporous carbon membranes prepared from resorcinol/formaldehyde polymer, *J. Membr. Sci.*, 2011, **379**(1–2), 52–59.

50 M. Yoshimune, K. Mizoguchi and K. Haraya, Alcohol dehydration by pervaporation using a carbon hollow fiber membrane derived from sulfonated poly(phenylene oxide), *J. Membr. Sci.*, 2013, **425**, 149–155.

51 G. Jyoti, A. Keshav and J. Anandkumar, Review on pervaporation: theory, membrane performance, and application to intensification of esterification reaction, *Journal of Engineering*, 2015, **2015**(2), 1–24.